Research Article | Vol. 1, No. 5 / 15 May 2022 / Optics Continuum 1098

OPTICS CONTINUUM

# Joint manifestation of quasi-phase-matching and resonance enhancement of harmonics in laser-induced plasmas

RASHID A. GANEEV,[1,2,3] VYACHESLAV V. KIM,[1,*] GANJABOY S. BOLTAEV,[3] IBROKHIM B. SAPAEV,[3] AND SERGEY Y. STREMOUKHOV[4,5]

[1] *Institute of Astronomy, University of Latvia, Riga, LV – 1586, Latvia*
[2] *Department of Physics, Voronezh State University, Voronezh 394006, Russia*
[3] *Tashkent Institute of Irrigation and Agricultural Mechanization Engineers, National Research University, Kori Niyozov street 39, Tashkent 100000, Uzbekistan*
[4] *Faculty of Physics, Moscow State University, Leninskie Gory, 1, build.2, Moscow, 119991, Russia*
[5] *Moscow Institute of Physics and Technology, 9 Institutskiy Lane, Moscow Region, Dolgoprudny 141701, Russia*
[*] *rashid_ganeev@mail.ru*

**Abstract:** We compare two processes (resonance enhancement and quasi-phase-matching) allowing the enhancement of the high-order harmonics of ultrashort pulses during propagation through different laser-induced plasmas (vanadium, antimony, indium, and manganese). We show how the tuning of maximally enhanced harmonics during quasi-phase-matching in multi-jet plasmas can enhance the resonantly-enhanced harmonics. Theoretical calculations support experimentally observed quasi-phase-matching of a group of harmonics and single harmonic enhancement.



## 1. Introduction

The high-order harmonics generation (HHG) in gases, laser-induced plasmas (LIP), and from surfaces attracts attention due to the formation of the sources of coherent radiation in the extreme ultraviolet (XUV) range and the generation of pulses on the attosecond time scale. Different processes can change the characteristics of HHG. Among them, single-harmonic enhancement (SHE) and quasi-phase-matching (QPM) of a group of harmonics are the most attractive methods for increasing the output of coherent radiation in the XUV.

Various groups studied different processes during experimental studies of HHG in LIP [1–11]. Additionally, the theoretical studies of the resonant effect on SHE were carried out using various approaches. Initially, the influence of multiple electron trajectories was assumed to cause this process during HHG in LIP [12]. Then, a four-step model considered the ion transitions with large oscillation strength (*gf*) between the ground state and the autoionizing state (AIS) of ions [13]. Other models were based on bound-bound transitions [14–16], as well as on the coupling of multi-electron excited states with increased harmonic output [17,18]. Each of these models to some extent confirms the described experiments with HHG related to the observation of the resonance effect in plasma. The four-step model [13] seems to be more convenient to provide the experimentally oriented numerical calculations. Notice that a search for transitions with large *gf*s gives a possibility to verify the optimal position of resonant harmonics in the HHG spectrum in the frames of the four-step model.

The same can be said about the compatibility of the theoretical explanations of QPM between driving and harmonic waves and the described experimental realizations of this process in gases and plasmas. HHG of laser radiation in extended gas media has long been considered an

#454617 https://doi.org/10.1364/OPTCON.454617
Journal © 2022 Received 25 Jan 2022; revised 7 Apr 2022; accepted 11 Apr 2022; published 3 May 2022

inefficient process due to the excess of the average length over the coherence length ($L_{\mathrm{coh}}$) of harmonics. At a distance equal to $L_{\mathrm{coh}}$, the phase mismatch π increases and causes destructive interference between the driving and harmonic waves. For gas harmonics in the XUV region, QPM is aimed at canceling out-of-phase radiation. As has been shown in several schemes of gas jets, as soon as the waves leave the medium, their phase changes [19–22]. Then the frequency conversion process can be effectively continued in another group of harmonic emitters.

The QPM effects in gas and plasma can be effectively simulated by the interference model [23] taking into account the single atom responses calculated using the non-perturbative approach [24]. In accordance to the interference model, the medium can be represented as a series of atoms interacting with a laser field having parameters depending on the position of the atom in the medium. Each atom emits the coherent radiation, which interferes (constructively or destructively) with the emission of other atoms. This model was used to study the QPM effects in plasma media [25] and gases [26].

In the case of LIP, the separation of the extended plasma plume into several small plasma jets can restore the correct phase ratio between the driving and harmonic waves and make it possible to further increase the harmonic yield in various spectral ranges of the XUV. Among the approaches for QPM in plasmas, the following methods can be considered: (a) the use of microlithographic targets, (b) the use of perforated targets that allow separation in time for the plasma jets to reach the axis of propagation of the driving beam, and (c) the use of multiple slits with different distances between them as screens installed in front of ablating targets, which makes it possible to achieve an adjustable separation between several plasma jets.

Meanwhile, the analysis of the joint application of two methods leading to harmonics enhancement was yet reported. There are no comparative studies of these micro- and macro-processes in the generation of high-order harmonics. Of particular interest is the joint manifestation of the advanced capabilities of SHE and QPM. Since the former process was previously implemented only in a plasma medium, the combination of these harmonic enhancement mechanisms can be demonstrated only in LIP. Here we presented the results of HHG studies in several LIPs under conditions when the two above processes complement each other. We show how the tuning of maximally enhanced harmonics during QPM in multi-jet plasma can further increase the resonantly enhanced single harmonic. Our theoretical calculations confirm the experimentally observed quasi-phase-matching of a group of harmonics and the enhancement of a single harmonic.

## 2. Experimental

Four metals (manganese, antimony, indium, and vanadium) were selected for these experiments. While various other ablated metals are suitable for demonstrating QPM in LIP, SHE is observed only in a limited number of plasma species. The QPM conditions in the selected ablated samples were created according to the scheme shown in Fig. 1(a).

The laser radiation was focused using a cylindrical lens on the surface of the above metals to obtain plasma in the form of an elongated line with a length of 5 mm (upper inset in Fig. 1(a)). Then a multi-slit mask (MSM) was inserted between the focusing cylindrical lens and the target to form a group of equally separated narrow laser beams that ignited a set of separated plasma jets (lower inset in Fig. 1(a)). The use of different fluencies and intensities of heating pulses made it possible to vary the characteristics of these narrow plasma jets, in particular, the particle density and the concentration of electrons ($N_{\mathrm{e}}$). These variations in plasma formation made it possible to match the sizes of plasma jets and the coherence length of the harmonics generated during propagation of the femtosecond pulses through a group of laser-induced jets. Images of ablated target areas in the case of a homogeneous extended linear laser beam and five narrow laser beams are shown in Figs. 1(b) and 1(c), respectively. The corresponding schemes for a

OPTICS CONTINUUM

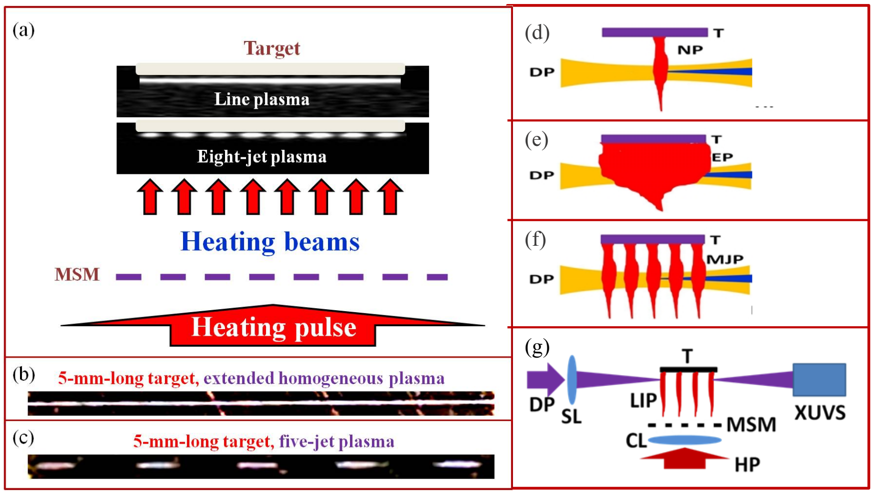


**Fig. 1.** Experimental arrangements for generation of QPM harmonics in LIP. (a) Ablation of extended targets by the heating pulses focused using a cylindrical lens. Extended imperforated LIP (upper raw image) and multi-jet LIP (bottom raw image) are shown. The latter plasma was formed by installing the multi-slit mask (MSM) on the path of the focused heating pulse. (b) Image of ablated surface in the case of line LIP. (c) Image of ablated surface in the case of the formation of five plasma jets. (d) Propagation of driving pulses (DP) through the single-jet narrow plasma (NP) formed on the target (T) surface. (e) Propagation of driving pulses through the extended plasma (EP). (f) Propagation of driving pulses through the multi-jet plasma (MJP). (g) Scheme for HHG in laser-induced plasmas. DP: driving pulses, SL: spherical lens, T: target, LIP: laser-induced plasma, XUVS: extreme ultraviolet spectrometer, MSM: multi-slit mask, CL: cylindrical lens, HP: heating pulses.

narrow single plasma jet, an extended plasma jet, and a five-jet structure are shown in Figs. 1(d), 1(e), and 1f, respectively.

Bulk manganese (Mn), vanadium (V), antimony (Sb), and indium (In) (Sigma-Aldrich) were placed in a vacuum chamber (Fig. 1 g) and ablated by different laser pulses to form LIP, with further HHG during the propagation of femtosecond laser pulses. The part of uncompressed radiation from a Ti: sapphire laser (central wavelength of 806 nm, pulse duration of 270 ps, pulse energy of 10 mJ, and a pulse repetition rate of 10 Hz) was used as a heating pulse for the target ablation. The heating pulse interacted with the target surface at normal incidence. The size of the focal spot on the target surface was maintained at 0.3 mm (in the case of focusing by spherical lens) and 0.3×5 mm (in the case of focusing by cylindrical lens).

The plasma density depends on the pulse duration and intensity (or rather fluence) of heating radiation, absorbance of materials, etc. Previous calculations based on the hydrodynamic code HYADES allowed determining the concentrations of electrons and plasma in the ablated plumes of different materials [27,28]. Particularly, this code allowed simulating the expansion of a silver slab interacting with a laser pulse and then determining the electron density, ionization level, and ion density as the functions of the heating pulse intensity at different distance from the target surface.

There are other methods of the determination of plasma characteristics. The particle concentration in the interaction zone can be determined by the thermodynamic parameters of the plasma. The absence of an abundance of ionized atoms under "mild" conditions of ablation was confirmed by spectral analysis of the plasma. In such a case, the thermal model with gas-dynamics boundary conditions can be applied for the analysis of the formation and heating of laser plasma [29]. Within the framework of this model, the vapor concentration and temperature are determined by the energy and flow conservation laws and saturated vapor concentration. The plasma density in the interaction zone was varied from $5\times10^{16}$ to $2\times10^{17}$ cm$^{-3}$, depending on the plasma sample, experimental conditions, and distance between the target and the laser beam. Additionally, to determine the density in the ablation plume a three-dimensional molecular dynamical simulation of laser ablation of materials can be performed using the open-source molecular dynamics code ITAP IMD [30,31]. Particularly, the density of the carbon plasma was calculated at the experimental conditions of target ablation (i.e., $2\times10^{10}$ Wcm$^{-2}$ in the case of 8-ps pulses and $1\times10^{9}$ Wcm$^{-2}$ in the case of 10-ns pulses) [32]. The corresponding densities were found to be $2.6\times10^{17}$ and $2.5\times10^{18}$ cm$^{-3}$. Obviously, it is hard to precisely determine the parameters of plasma for the definition of the optimal conditions for QPM. In our case, the estimated plasma density was $2\times10^{17}$ cm$^{-3}$.

The focused 50 fs pulses propagated through the LIP at a distance of 0.15 mm above the target surface. This distance is too small to allow the plasma expand largely towards the orthogonal direction. Correspondingly, the sizes of plasma jets through which femtosecond pulses propagate were almost equal to the sizes of the open parts of the multi-slit mask. The intensity of the focused 806 nm driving pulses inside the LIP was $3.5\times10^{14}$ W cm$^{-2}$. The two-color pump (TCP; 806 nm and 403 nm) was used to generate the odd and even harmonics, alongside the application of the single-color pump (SCP; 806 nm) of plasmas. A 0.2 mm-thick beta-barium borate (BBO, $\lambda = 403$ nm, 3% conversion efficiency) crystal was inserted into the vacuum chamber in the path of the focused 806 nm driving pulses to generate a second harmonic.

We directly measured the energies of the fundamental radiation and its second harmonic behind the crystal using the energy meter and corresponding calibrated filters. The broadening of second harmonic (SH) pulses compared with the fundamental radiation and the delay between these pulses can be determined using the relations

$$\tau_{2\omega} = [(\Delta_{delay})^2 + 0.5(\tau_\omega)^2]^{1/2} \tag{1}$$

$$\Delta_{delay} = d\left[\frac{1}{v_\omega} - \frac{1}{v_{2\omega}}\right]. \tag{2}$$

Here $t_{2\omega}$ is the pulse duration of SH after propagation of the fundamental pulse through the barium borate (BBO) crystal of the thickness of $d$, $t_\omega$ is the pulse duration of the fundamental radiation, and $v_\omega$ and $v_{2\omega}$ are the group velocities of the ordinary fundamental and extraordinary SH pulses, respectively. The pulse durations of fundamental and SH pulses were 50 and 67 fs. The sizes of these focused beams were approximately equal to each other.

Based on above-described measurements, we estimated the approximately rate of intensities in the case of single-color pump and two-color pump as 1:0.8. The most important uncertainty was a ratio of the overlap of two pulses in the plasma area. Even at these unfavorable conditions, the harmonic yields and extension of plateau were notably better in the case of the two-color pump. We did not made the comparative measurements of the two- and single-color pump induced HHG, since this topic was out of the main goal of this study. However, numerous publications, both during gas HHG and plasma HHG, demonstrated the advantages of the former approach.

We also used an optical parametric amplifier (OPA) to apply the tunable (1200-1400 nm) near infrared (NIR) driving pulses for HHG in the LIP. The signal pulses from the OPA (for example, 0.8 mJ, 80 fs, 1280 nm) were delayed by ~80 ns relative to the heating pulses using an optical delay line to adjust the moment of propagation of the driving pulses over the target surface at the moment when the plasma concentration was maximal. The intensity of the focused NIR driving pulses inside the LIP was $2\times10^{14}$ W cm$^{-2}$. The TCP of the LIP was also used in that case to apply the NIR and second harmonic (H2) pulses for the HHG in the plasmas. The harmonic radiation was analyzed using a homemade XUV spectrometer.

To create QPM conditions, one has to maintain a phase coupling between the driving and harmonic waves along the whole period of propagation through the generating medium. For a given size of a separate plasma jet (~0.5 mm in the case of a mask with 5 slits and an ablating target with a length of 5 mm), the QPM for the $q$th harmonic can be maintained at a fixed product $q{\times}N_e$, since

$$L_{\text{coh}} \approx 1.4 \times 10^{18} (\text{q} \times N_e)^{-1} \tag{3}$$

in the case of an 800 nm driving wave [33,34]. Here $L_{\text{coh}}$ is the coherence length (in mm), $q$ is the harmonic order in the QPM region showing the highest enhancement, and $N_e$ is the electron density in the plasma jets measured in $\text{cm}^{-3}$.

A decrease in $N_e$ with a weaker ablation of the target using lower heating pulse fluencies should lead to an optimization of QPM for a higher $q$ in order to preserve the product $q \times N_e$ unchanged for fixed spatial characteristics of plasma jets. We used MSMs with different widths of slits (0.2, 0.3, 0.5, 0.6 and 0.8 mm). The distance between the slits was equal to the width of the slits. The use of various MSMs allowed us to optimize the spectral range of the enhanced group of harmonics centered on the maximally enhanced harmonic order ($q_{\max}$), the coherence length of which was equal to the width of one slit.

We used the same intensity of the heating pulses in both cases (without and with multi-slit mask) for the same material. However, this intensity was different for the four targets due to the obvious difference in the creation of the optimal LIP.

## 3. Joint involvement of resonance and QPM processes

### 3.1. Vanadium plasma

Previously, HHG in vanadium plasma made it possible to achieve an expansion of the harmonic cutoff to the 71st order of pumping 800 nm radiation with an efficiency of harmonic generation in the plateau range of $1.6{\times}10^{-7}$ [35]. Meanwhile, only low-order harmonics (up to the 23rd order) were obtained when the vanadium target became weakly excited.

In our experiments with vanadium plasma, when excited using a larger fluence and intensity of heating pulses ($I_{\text{hp}}$ “ $4{\times}10^{10}$ W $\text{cm}^{-2}$), the harmonics of 806 nm pulses up to H35 were achieved. In the case of imperforated LIP (upper panel of Fig. 2(e)), we show a decay of all harmonics towards the cut-off region (H39; this harmonic is seen in the raw image shown in Fig. 2(a), though less visible in the lineout shown in Fig. 2(e)) for the vanadium plasma. This is an obvious pattern of all harmonic spectra. The difference is the unusually strong H27 (see also Fig. 2(a)), which is attributed to the involvement of the resonance-induced enhancement of this harmonic. In the case of a single-jet LIP ($l = 0.5$ mm, Fig. 2(a)), the strong 27th harmonic dominated in the spectral range of 20-37 nm due to the influence of a strong but unidentified ion transition with a large $gf$.

The enhancement of single harmonic occurs due to the closeness of this harmonic to the AIS possessing large oscillator strength. Previous empirical observations of the harmonics in the plateau region, which significantly exceed the neighbor ones, found the theoretical confirmation in a few studies [13,17,36,37]. Occasionally, previous measurements of the oscillator strengths of those transitions almost perfectly coincided with what was observed in experiment (for example, in the case of indium plasma during generation of strong 13$^{\text{th}}$ harmonic of 800 radiation). Most of observed enhanced harmonics were identified as being close to the reported strong ionic transitions. Meanwhile, some of them were not identified, particularly, the ionic transition of vanadium in the vicinity of the 27$^{\text{th}}$ harmonic of 800 nm radiation. To the best of our knowledge, there are no reports in the journals and information in the databases of NIST, etc. regarding the strong ionic transition of V at ~29 nm. A lack of knowledge of the spectroscopic properties of this metal in XUV just points out the advantage of HHG in LIPs allowing determining such transitions by the empirical method.

OPTICS CONTINUUM

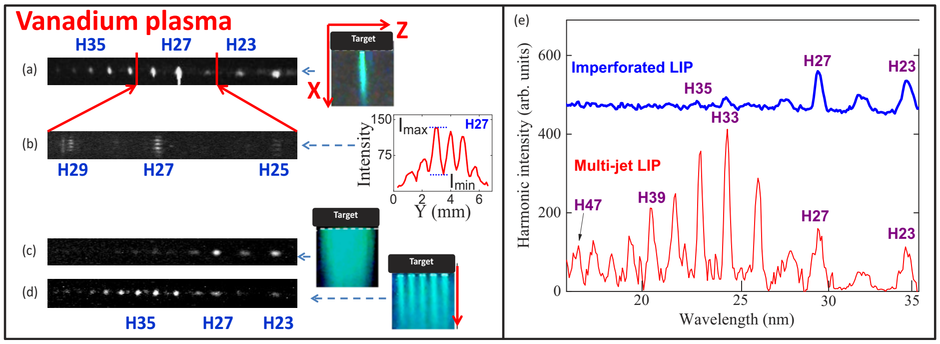


**Fig. 2.** Harmonic spectra from vanadium plasma. (a) Raw images of harmonic spectra were obtained during HHG of 806 nm pulses in narrow LIP ($l = 0.5$ mm). 21$^{st}$ to 37$^{th}$ harmonics are presented, with strong H27. Inset: the shape of narrow plasma. (b) Images of interference patterns of H25 – H29 were obtained using a double-slit configuration. Inset: spatial distribution of the interference pattern of H27 (see text). (c) HHG in extended LIP. The comparable intensities of 23$^{rd}$ and H27th harmonics were obtained. Inset: the shape of extended 5-mm-long plasma. (d) HHG in multi-jet LIP. One can see a significant growth of H31-H39 and decay of H27. Inset: the shape of 5-jet plasma. (e) Spectral distribution of the harmonics generated in extended imperforated vanadium plasma (upper curve) and multi-jet LIP (bottom curve). The accumulated number of laser shots was 10.

The degree of spatial coherence of the harmonics generated in LIPs is an important parameter in applications requiring high spatial coherence. Resonantly enhanced harmonics can have either low or high spatial coherence, depending on the HHG conditions in the plasma. We analyzed this parameter in the case of resonantly enhanced H27 (Fig. 2(b)). The test for the coherent character of the emission from vanadium plasma was carried out using a Young double-slit interferometer. The double slits were mounted on a translation stage and placed approximately 40 cm from the targets, with the microchannel plate of XUV spectrometer positioned at 70 cm from the slits. The two slits, spaced by 25 µm, were made from stainless steel and had 8 µm width and 10 mm length. A flat field grating, a microchannel plate, and a CCD camera of an XUV spectrometer were used to analyze the images of interference fringes.

The fringe visibility was determined by the ratio $V = (I_{max}-I_{min})/(I_{max}+I_{min})$, where $I_{max}$ and $I_{min}$ correspond to the maximum and minimum intensities of the interference pattern (right inset in Fig. 2(b)). In the case of H27, the measured visibility of the fringes corresponding to the modulus of the complex coherence coefficient in the case of H27 was determined as $V = 0.61$. We observed approximate equality in the visibility of the fringes from resonant (H27) and non-resonant (in particular, H25 and H29) harmonics. This parameter depends, in particular, on the value of $N_e$, which can reduce V in highly excited plasmas and gases.

We did not see similar coherence properties of the spontaneous emission from the vanadium plasma at the same spectral region by overexciting the target using strong heating pulses. Those experiments showed weak visibility of the interference fringes in the case of spontaneous emission of laser-induced plasma, while the visibility of harmonics-induced interference pattern (~0.65) was almost similar to the case of the optimal plasma formation. This measurement is related to the "non-optimal" plasma formation, i.e. plasma formed at stronger ablation of targets. Our studies showed that the coherency of harmonics defined from the visibility of interference pattern of harmonics did not significantly vary at different conditions of plasma formation. The difference of V between these two conditions of plasma formation was in the range of the accuracy of measurements of this parameter (±0.5). Thus the interference tests confirmed that the observed radiation of harmonics from the vanadium ablation plume possesses good coherence for both resonance-enhanced harmonic (H27) and neighboring unenhanced harmonics (H25 and N29).

We carried out these measurements of a single randomly chosen resonance-enhanced harmonic in the case of one of four samples to show the coherence properties of the generated radiation. Obviously, it is not necessary to measure the visibility of all harmonics from all targets to demonstrate the generality of the high coherency of this radiation. Notice that there is no relation between the linewidth and coherency properties of harmonics, at least for the used range of driving pulses intensity.

The formation of extended vanadium plasma (right inset in Fig. 2(c)) led to a decrease in the output of harmonics above H27, which made it possible to emphasize the enhancement of this harmonic with respect to all neighboring orders (see the original image of the harmonic spectrum shown in Fig. 2(c)). The lineout of this figure is shown in Fig. 2(e) (upper curve). Weak decayed harmonics can be seen in the range of 22 - 28 nm (i.e. below the wavelength of the resonantly enhanced H27, $\lambda = 29.6$ nm), with almost no harmonic radiation below this region of the spectrum. The decrease in the output of higher-order harmonics in the case of extended plasma was associated with lower coherence lengths of these harmonics compared to the length of the extended plasma (5 mm) under the conditions of plasma formation used.

This pattern of harmonic distribution changed dramatically as soon as multi-jet plasma consisting of five 0.5 mm long jets separated by 0.5 mm from each other was created on the target surface. The image of the formed LIP diverging from the surface of the vanadium target is shown in the left inset of Fig. 2(d). A relatively small divergence of these plasma jets is visible, which allows expecting the distance between them to remain approximately the same (~0.5 mm) at a distance of 0.2 mm from the target surface. The raw image of the harmonic spectrum (Fig. 2(d)) demonstrates a notable enhancement of the harmonics exceeding those orders observed in the imperforated plasma (Fig. 2(c)).

The dominance of H33 and H35, the extension of the enhanced harmonics up to the 53rd order (not shown in this figure) and the relative decrease in the enhancement of the resonance-affected H27 compared to the group of harmonics improved by QPM were among the notable changes visible on the screen of the CCD camera capturing the images of harmonics distribution. The lineout of this spectrum (the lower curve of Fig. 2(e)) in the case of a five-jet plasma confirms the predominance of a group of harmonics with QPM enhancement over a resonantly enhanced single harmonic. The discrepancy in the wavelengths of maximally enhanced QPM harmonic and SHE did not allow achieving an additional increase in the output of the latter harmonic. Moreover, due to the location of this harmonic on the wing of the gain caused by QPM, we observed only a 1.5-fold increase in H27, while the neighboring H29 was increased by 4.2 times (compare the upper and lower curves in Fig. 2(e)). Meanwhile, a gain of 11.5× was achieved in the case of $q_{\max}$ (H33).

### 3.2. *Antimony plasma*

The formation of conditions for the coincidence of the maximally enhanced harmonics in two processes (SHE and QPM) requires the use of the LIP, which allows generating the highest possible order of resonance-enhanced harmonic. One of the examples of such plasmas can be an antimony LIP. To analyze the conditions under which the above coincidence can be realized, we used the single-color (1310 nm) and two-color (1310 nm + 655 nm) pumping of plasma. The latest pump configuration of the antimony plasma allowed us to observe the increased outputs of SHE (H35) emission and QPM in the same spectral region.

Figure 3(a) shows the harmonic spectra in the case of single-color (red thick curve) and two-color (blue thin curve) pumps of a narrow (0.4 mm) LIP. In the first case, only a few odd harmonics of 1310 nm radiation, up to H31 in the spectral range of 32–48 nm, were observed. The two-color pump (1310 nm + 655 nm) allowed us to generate a plateau-like distribution of odd and even harmonics up to H38. The strong H35 ($\lambda = 37.4$ nm, gain ~5 relative to the neighboring harmonics) dominated over other odd and even harmonics. In this case, a near coincidence of H35 with strong transitions of Sb II ions was attributed to SHE.

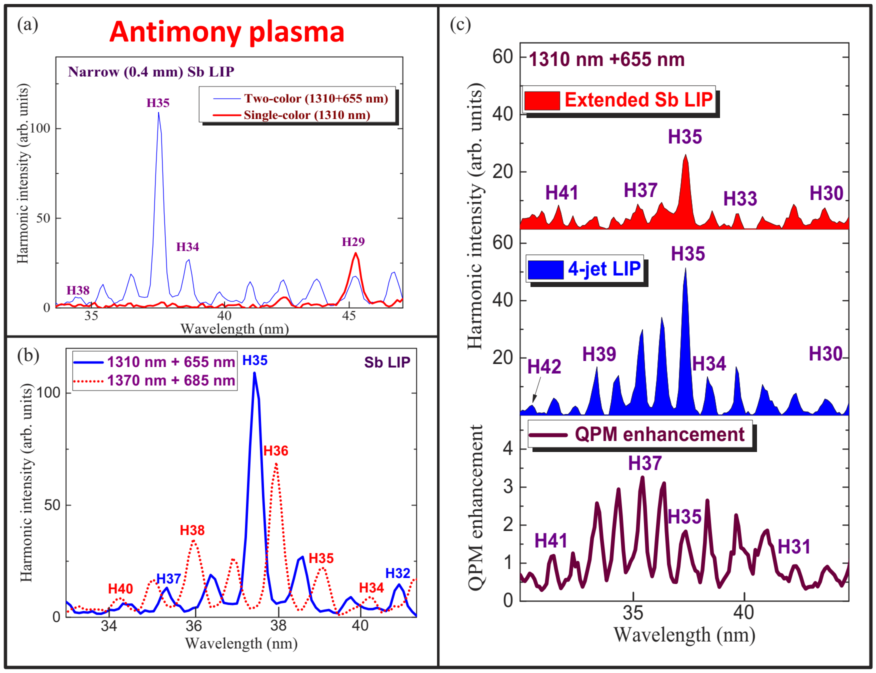


**Fig. 3.** Harmonic emission from antimony plasma. (a) Two-color (1310 nm + 655 nm, blue curve) pump and single-color (1310 nm, red color) pump of narrow (0.4 mm) Sb LIP. (b) Modification of harmonic emission in the vicinity of strong resonance transition of SbII using the tuning of near-infrared pulses. Blue solid curve: 1310 nm + 655 nm pump. Red dotted curve: 1370 nm + 685 nm pump. (c) Harmonic spectra and enhancement during two-color pump of extended Sb plasma. Upper panel: extended (5 mm) imperforated Sb LIP. Middle panel: HHG in four-jet LIP. Bottom panel: QPM-induced enhancement factors of the group of harmonics. The accumulated number of laser shots was 10. The arbitrary units are different for (a) – (c) panels and are used for comparative purposes in each of those panels.

Previously, a 10-fold enhancement of a single high-order harmonic near the $4d^{10}5s^22p^3P_2 - 4d^95s^25p^3(^2D)^3D_3$ transition of SbII ($\lambda = 37.82$ nm) in the case of a low-ionized antimony plume was reported [38]. The conversion efficiency of this harmonic was $2.5\times10^{-5}$, and the output energy was 0.3 µJ. The used excitation pulses (795 nm) made it possible to increase H21 ($\lambda = 37.7$ nm) yield from a narrow Sb plasma.

Antimony has two strong ionic transitions ($4d^{10}5s^22p^3P_2 - 4d^95s^25p^3(^2D)^3D_3$ and $4d^{10}5s^22p^1D_2 - 4d^95s^25p^3(^2D)^3F_3$) in the vicinity of 37 nm [39]. The *gf*s of these transitions were calculated as 1.36 and 1.63, respectively, which is 6-7 times higher than those of neighboring transitions. The reason for the different enhancement of the H21 pump with a wavelength of 795 nm (10×, [38]) and the H35 pump with a wavelength of 1310 nm (5×) can be probably attributed to the proximity of the $4d^{10}5s^22p^3P_2 - 4d^95s^25p^3(^2D)^3D_3$ transition driven by the AC Stark shift and the former harmonic. It is difficult to argue about the comparative involvement of this effect on the tuning of the transitions under consideration towards the harmonic wavelength. Moreover, there is no need in the exact coincidence of the wavelengths of ionic transition and harmonic to achieve the maximum growth of harmonic yield.

OPTICS CONTINUUM

Tuning the wavelength of the optical parametric amplifier allowed us to demonstrate a change in the order of the maximally enhanced harmonic. In particular, in the case of a pump of 1370 nm + 685 nm, the maximum increased harmonic order was set to H36 (Fig. 3(b), red dotted curve; compare with H35, the blue solid curve for a pump of 1310 nm + 655 nm). The gain of this harmonic was lower than that of H35, which was explained by the better phase-matching conditions in the latter case.

In the case of an elongated (5 mm) Sb LIP, a single-color pump (1310 nm) allowed us to generate harmonics up to H41 (Fig. 3(c), upper panel). The use of MSM containing slits with a width of 0.6 mm made it possible to form four jets with a width of 0.6 mm, separated from each other by 0.6 mm instead of a 5 mm-long imperforated LIP. In this case, the maximally enhanced group of harmonics (H36 and H37) was close to the H35 enhanced due to the closeness with the strong ionic transition of SbII (Fig. 3(c), middle panel). The QPM-induced enhancement of these harmonics was calculated by dividing the blue curve (middle panel) by the red curve (upper panel). On the lower panel of Fig. 3(c), one can see the gain coefficients of all harmonics in the spectral range of 30-45 nm. It is possible to assume a smaller gain of the "resonant" (H35) harmonic in comparison with neighboring ones. This decrease in the gain of the H35 harmonics can be explained by the above-mentioned stronger influence of free electrons on the phase-matching conditions of the resonantly-enhanced single harmonic compared to the QPM-enhanced group of harmonics.

### 3.3. Indium plasma

The plasma from this metal was used as an effective sample for SHE in the vicinity of a very strong transition of InII ($\lambda = 62.24$ nm, $gf = 1.11$ [40]). The first observation of this effect [12 28] allowing the generation of exceptionally strong H13 of 800 nm laser was accompanied by an analysis of this process both theoretically [13 29] and experimentally [41].

The joint manifestation of SHE and QPM is aimed at demonstrating the comparison of these two processes lying in different spectral ranges. The harmonic (H21, $\lambda = 62.86$ nm) resonantly enhanced in the case of pumping by 1320 nm + 660 nm pulses of extended indium plasma and the expected maximally enhanced group of harmonics centered at about the thirtieth harmonics (35–42 nm) do not affect each other. Our studies of this process revealed some new features of the relative enhancement factors associated with the above processes.

The raw image shown in the upper panel of Fig. 4(a) represents the distribution of harmonics generating in the extended (5 mm) In LIP. The main peculiarity here is a very strong H21 followed by very weak higher-order harmonics, which are barely seen and extended up to the 39$^{th}$ order. The insertion of the MSM with the slit sizes of 0.6 mm on the path of the heating pulses allowed us the formation of four jets on the 5-mm-long target. This manipulation with the shape of homogeneous LIP led to the formation of the optimal conditions for the significant enhancement of the harmonics centered at around H33 (bottom panel of Fig. 4(a)). The visual observation of the harmonics distribution demonstrates how the coherent addition of the harmonic yield in the 30–50 nm range led to the formation of conditions when the coherence length of H33 coincided with the width of the single jet at the fixed $N_e$ inside the indium plasma.

The quantitative presentation of this effect in the 25–55 nm spectral range in the case of 1300 nm + 650 nm two-color pump of In LIP is seen in Fig. 4(b). The upper panel shows the plateau-like shape of weak harmonics distribution up to H40 in the case of imperforated plasma. The ratio between the resonantly enhanced 21$^{st}$ harmonic and ordinary harmonic in the plateau range (for example, H29) was quite large (~27) thus demonstrating the dominance of the SHE effect at these conditions. The insertion of MSM with six 0.4-mm-long slits allowed us the formation of six jets leading to the enhancement of harmonics in the 35 nm region (middle panel). At these conditions of plasma modulation, the ratio of resonance- and QPM-enhanced harmonics became significantly lower (H21/H38 = 3.7). Even closer intensities of the resonance and QPM

OPTICS CONTINUUM

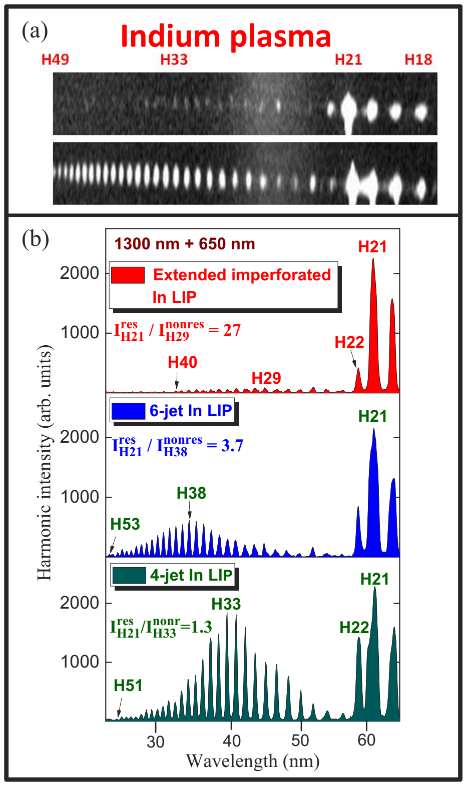


**Fig. 4.** HHG in indium LIP. (a) Raw images of harmonic spectra generated in the indium LIP pumped by 1320 nm + 660 nm pulses. The upper spectrum corresponds to the HHG from the homogeneous extended indium plasma. The bottom spectrum corresponds to the HHG from the multi-jet indium LIP with the single plasma jet sizes of 0.6 mm. (b) Harmonic spectra line-outs from indium LIP in the 25–65 nm spectral range using different configurations of laser-plasma. Upper panel: extended (6 mm) imperforated LIP. The ratio between resonance harmonic (H21) and plateau harmonic (H29) is 27. Middle panel: six-jet LIP. The ratio between resonance harmonic (H21) and maximally QPM-enhanced harmonic (H38) is 3.7. Bottom panel: four-jet LIP. The ratio between resonance harmonic (H21) and maximally QPM-enhanced harmonic (H33) is 1.3. The accumulated number of laser shots was 10.

OPTICS CONTINUUM

harmonics were achieved in the case of four plasma jets formed using the MSM containing the 0.6-mm-long slits. In that case, the envelope of enhanced harmonics was shifted towards the longer-wavelength region (~40 nm, Fig. 4(b), bottom panel). At these conditions of plasma modulation, the H21/H33 ratio was close to 1.3, thus demonstrating the approximate equality in the enhancement factors of SHE and QPM. Notice that the enhancement of other harmonics in this spectral range implies a significant growth of the integrated yield of coherent radiation in the shorter-wavelength region.

The variation of H21, as well as lower-order harmonics, in the case of imperforated and multi-jet plasmas was almost insignificant (compare the raw images of those harmonics in Fig. 4(a) and the relative intensities of H21 in Fig. 4(b)), which underline a small influence of QPM on the harmonics lying far from the spectral region affected by the multi-particles related process.

### 3.4. Manganese plasma

Manganese plasma allows generating the highest orders of harmonics reported so far in the case of HHG in LIPs. One of the features of this medium is the appearance of a "second plateau" in the distribution of harmonics, as soon as the plasma becomes properly formed and excited. The second plateau appears in the region below 24 nm to ~8 nm. The beginning of this plateau corresponds to the strong resonantly enhanced 33$^{rd}$ harmonic of the Ti:sapphire laser ($\lambda = 24.4$ nm; the red dotted curve in Fig. 5(a)). This observation is consistent with the data presented in the case of single-color pumping of the Mn LIP by 800 nm class lasers [42–44]. The use of a two-color pump (806 nm + 403 nm) made it possible to generate a stronger even harmonic in this area (H34; Fig. 5(a), solid blue line). In both cases of pumping, the 24 nm region becomes generating the strongest harmonics in the spectral range below $\lambda = 37$ nm.

Previously, the optimal enhancement conditions for H33 of 800 nm laser in the vicinity of giant 3p-3d resonances of Mn II in the range of 23.8–24.3 nm, which is the region of the metastable states of manganese [45], were controlled by various means [46]. An increase in the fluence of the heating pulse led to an increase in the plasma concentration, which is an important factor for improving the harmonic output due to a larger number of emitters. However, along with the growth of plasma density, the predominant influence of free electrons appearing with stronger ablation on the phase-matching conditions leads to the cancellation of the optimal phase relations between the interacting waves. Accordingly, the growing phase mismatch leads to a decrease in the harmonic cutoff. This process becomes predominant in the case of an extended manganese LIP, when only weak harmonics up to H51 are generated in such plasma (Fig. 5(b), red dotted curve). To eliminate the influence of hindering factors, we changed the shape of an imperforated manganese plasma creating a six-jet LIP with a single jet size of ~0.4 mm. Under these conditions, a strong enhancement of a group of harmonics with a center near H43 was observed (Fig. 5(b), blue solid curve). It can be seen that the improvement attributed to QPM was stronger than the improvement associated with SHE. Moreover, a comparison of the H33 in these two cases shows almost the same output, while the nearby higher-order harmonic (H35) was increased by 4 times.

A decrease in the fluence of heating pulses made it possible to improve the propagation of harmonics in imperforated extended plasma (up to H69, not shown in Fig. 5(c), red dotted curve). Another MSM was installed to form eight jets with a single jet size of ~0.3 mm in order to expand the enhancement of weak harmonics in the 12–20 nm spectral range. The blue solid curve in Fig. 5(c) shows a drastic increase of harmonics output in this region caused by the formation of QPM conditions, in addition to the region where the harmonic with resonance enhancement prevails over other orders (~24 nm). The maximum output was observed for H55 (gain ~8×). One can clearly see a larger output of several harmonics at around this maximally enhanced QPM harmonic compared to the resonantly enhanced H33 harmonic.

OPTICS CONTINUUM

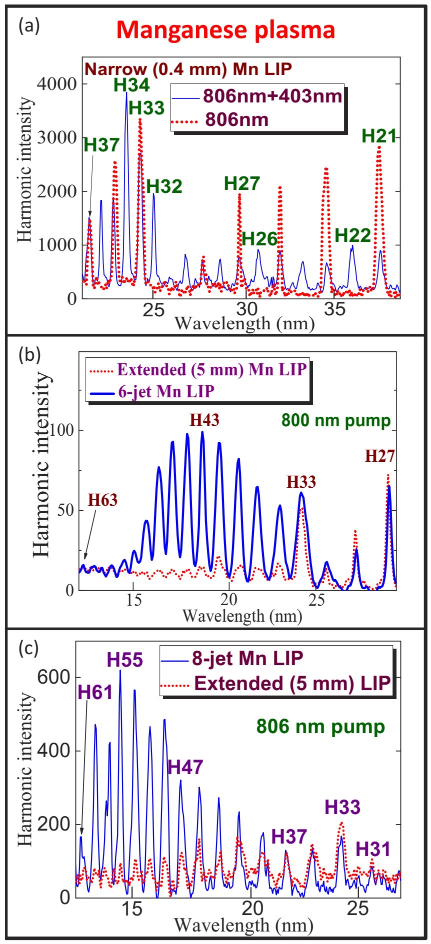


**Fig. 5.** Harmonic line-outs from manganese plasma in the case of HHG using SCP (806 nm) and TCP (806 nm + 403 nm). (a) Single-color (red dotted curve) and two-color (blue solid curve) pumps of narrow (0.4 mm) Mn LIP. (b) Harmonic spectra from extended imperforated Mn LIP (red dotted curve) and 6-jet plasma (blue solid curve). (c) Harmonic spectra from extended imperforated Mn LIP (red dotted curve) and 8-jet plasma (blue solid curve). The accumulated number of laser shots was 10. The arbitrary units are different for (a) – (c) panels and are used for comparative purposes in each of those panels.

## 4. Theoretical consideration of the joint manifestation of SHE and QPM

As discussed above, SHE, which arises due to large oscillator strengths of the transitions between ground states and AIS of ions in the plasma, can be well interpreted within the framework of the "four-step model" [13,47]. The output of enhanced harmonics depends on the number of emitters. As a result, the intensity of the enhanced harmonics should be reduced when replacing the extended plasma with a perforated one due to a twofold reduction in the number of ions in this case. The decrease in intensity of "resonance" harmonics at QPM conditions was experimentally determined in the manganese and indium plasmas (Fig. 5(c) and 4(a), respectively), while in two other studied LIPs (Sb and V), an increase in the intensity of resonantly enhanced harmonics was observed under QPM conditions.

This difference is explained by the degree of overlap of the spectral positions of a group of QPM-enhanced harmonics and a resonance-enhanced single harmonic. In particular, in the case of 8 jets of manganese plasma, the position of harmonics with QPM enhancement (centered at around H55) is quite far from the resonant (H33) harmonic (Fig. 5(c)). The same can be said about HHG in indium plasma (Fig. 4(a)). Meanwhile, in the other two cases (vanadium and antimony plasmas), the QPM in LIPs increases the output of the resonant harmonic to some extent (Figs. 2 and 3).

Overall, a significant increase of SHE in the LIP was not achieved under the QPM conditions while using the multi-jet plasma. The lack of strong enhancement may be due to the balance of two factors: a decrease in the number of emitters in multi-jet plasma compared to an extended plasma, which reduces the influence of SHE, and QPM-induced increase of the intensity of single resonance-enhanced harmonic.

To study the QPM phenomenon in LIP independently of SHE, we performed the numerical calculations of QPM-enhanced harmonics in the vanadium, antimony, indium, and manganese plasmas and compared these calculations with experimental data. The calculations were carried out within the framework of the interference model [23] and the nonperturbative approach [24]. As it was mentioned in introduction section, within the framework of the theoretical description of the plasma photoemission reaction, the medium was represented as a series of atoms interacting with a laser field, having parameters depending on the position of the atom in the medium. Due to the propagation in the medium, the parameters of the laser field change from atom to atom. The response of individual atoms is calculated in the framework of the nonperturbative theory [24] (amplitudes and phases of harmonics and its dependencies over the position of the atoms inside the LIP extracts from numerical experiments). The total response of the photoemission of the medium is calculated in accordance with the interference model (as a sum of coherently generated emitters) [23]. The parameters of the laser fields (intensities of single and two-color laser field components, their temporal widths, and delay times between the components of two-color laser fields) and the plasma parameters (such as widths of LIP jets, their number, densities of plasmas) were selected in accordance with the experimental data.

We assume that parameters of the laser field change during the propagation in the LIP due to dispersion. The influence of plasma is taken into account in accordance with the Lorentz theory [25,48]. Reabsorption of the generated radiation is not taken into account.

Here we show how the parameters of interaction are used in the numerical calculations in the case of the indium 6-jets LIP. Due to QPM the maximally enhanced harmonic order is 40. In accordance with Eq. (3) $N_e = 8.4\times10^{16}$ cm$^{-3}$, total plasma density is $2\times10^{17}$ cm$^{-3}$. In accordance with the Lorentz classical theory the refractive indices of plasma at $\lambda_1 = 1320$ nm and $\lambda_2 = 660$ nm were calculated. The initial ~30 fs delay between two pulses (due to passing through the 0.2 mm thick BBO crystal) increases along the propagation through the plasma. Those parameters are used to calculate the harmonics parameters in the case of the ensemble of In atoms placed in plasma.

OPTICS CONTINUUM

The results of numerical calculations of the QPM enhancement of harmonics in the four studied plasmas are shown in Figs. 6 and 7 (indicated by stars). The experimentally measured QPM enhancements are also shown in Figs. 6 and 7 for direct comparison (indicated by squares). The positions of the maximally enhanced harmonics calculated numerically and measured experimentally, almost coincide with each other. Moreover, the calculated values of the QPM enhancement also correspond to the experimentally measured ones. The results of numerical calculations allow us to separate the influence of QPM and SHE: in all calculated cases, the influence of QPM on the resonance-enhanced harmonic is constructive (except for the case of 8-jets manganese plasma presented in Fig. 7(b) by red circles and 4-jets indium plasma presented in Fig. 7(a) by red circles). As a result, in most cases, the decrease in the number of ions is compensated by a small addition of QPM-induced enhancement of "resonance" harmonics. The latter makes it possible to observe a slight growth of the harmonics enhanced by resonance in all cases, except for the case of 8 jets of manganese plasma and for both investigated cases of indium

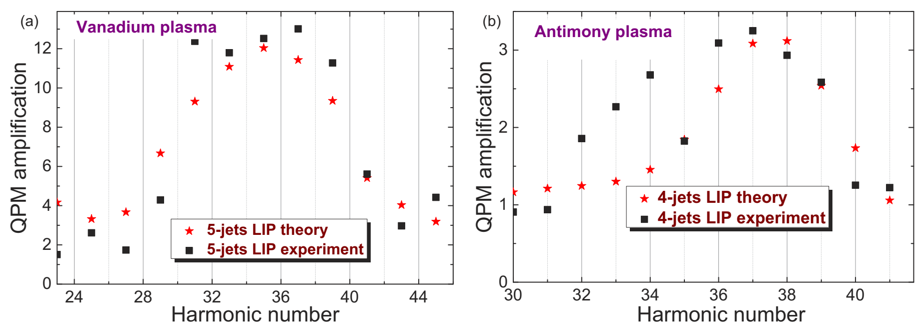


**Fig. 6.** (a) Calculation of QPM enhancement in vanadium plasma presented in Fig. 2(d) in the case of perforated plasma (red stars). Experimentally measured QPM enhancement is presented for comparison (black squares). (b) Calculation of QPM enhancement in antimony plasma presented in Fig. 3(c), bottom panel (red stars). Experimentally measured QPM enhancement is presented for comparison (black squares).

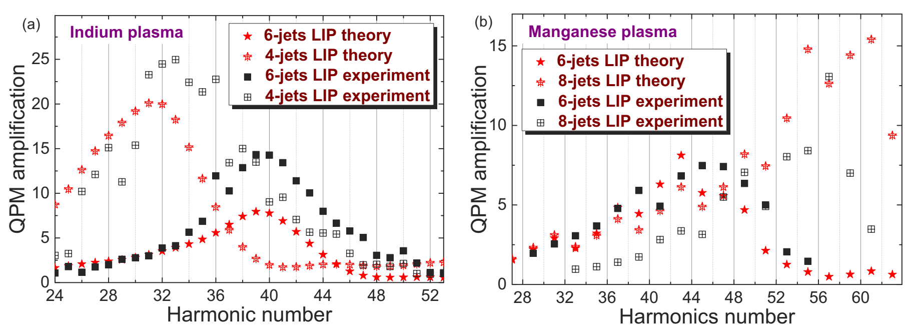


**Fig. 7.** (a) Calculation of QPM enhancement in indium plasma presented in Fig. 4(b), middle panel (red stars) and Fig. 4(b), bottom panel (red open crossed stars). Experimentally measured QPM enhancement is presented for comparison by black squares (from Fig. 4(b), middle panel) and by black open crossed squares (from Fig. 4(b), bottom panel). (b) Calculation of QPM enhancement in manganese plasma presented in Fig. 5(b) (red stars) and Fig. 5(c) (red open crossed stars). Experimentally measured QPM enhancement is presented for comparison by black squares (from Fig. 5(b)) and by black open crossed squares (Fig. 5(c)).

OPTICS CONTINUUM

plasma, since the position of maximally enhanced QPM harmonics for these cases are far away from the “resonant” harmonics for these types of plasma.

## 5. Discussion

Below we address the rational in choosing the targets for ablation. HHG can be realized in various plasmas; however not all of them are suitable for the goals of our study. For example, aluminum plasma allows generation of weak harmonics. Additionally, it does not provide the opportunity in demonstration of the resonance enhancement of single harmonic. The latter is one of the topics of present studies aimed in comparison of the effects of (a) a microprocess related to the single particle response leading to the enhancement of a single harmonic due to its vicinity to the strong transitions, i.e. those possessing high values of oscillator strength, and (b) a macroprocess related to the collective response of a whole medium allowing the formation of the artificially created phase-matching between the fundamental wave and the waves of a group of harmonics. Correspondingly, neither Al, nor many other materials are suitable for the comparative studies of the abovementioned processes. Notice that most suitable metal for efficient HHG in LIP is silver, which provides exceptionally strong harmonics along a broad range of XUV and extremely useful for the demonstration of QPM. However, the LIP produced on the surface of this metal does not allow generation of the resonance-induced single harmonic and correspondingly cannot be used for our goal.

Firstly, we have chosen the plasmas allowing the resonance-induced generation of single harmonic. Currently those are Cr, Mo, Sn, Te, As, Sb, V, In, and Mn. Among them four latter species are most compatible for our task of the comparative QPM/resonance studies. Other metals (Cr, Mo, Sn, Te, As) are less suitable from the point of view of the formation of the extended plateau of harmonics, which is a prerequisite for the observation of the QPM effect in different regions of XUV.

Thus the general meaning of our findings in view of other materials is the necessity to choose the appropriate plasmas allowing simultaneous observation of two processes overlapping with each other. Our choice of four materials (Sb, Mn, In, and V) allowed demonstrating the effects of joint involvement of two abovementioned processes in the increase of the harmonic yield.

The routine to demonstrate these processes was as follows. Firstly, we created the extended plasma on the surfaces of those targets. The conditions of the formed plasma did not correspond to the maximal yield of harmonics. This is explained by the over-excitation of the target leading to the formation of a large amount of the free electrons in plasma alongside the denser plasma. Large concentration of electrons caused the phase-mismatch between the interacting waves during propagation of a short distance inside such plasma due to the shortened coherence length for the harmonics, especially those belonging to the shorter-wavelength range. To constructively combine the yield of harmonics generation one has to maintain the distance of plasma corresponding to the coherence length of those harmonics. In that case the flip of the phase difference between the fundamental wave and the waves of the group of harmonics (not a single one, since the spectral dispersion of plasma changes slowly) after propagation of the short distance prevents the destructive conversion of harmonics back to the fundamental wave. Secondly, the formation of “dashed” plasma is produced by inserting the multi-slit mask just after the cylindrical lens allowing the formation of a line focus.

The basics of this approach are as follow. An alternative to perfect phase matching is classical QPM in periodically poled structures, where the nonlinear polarization axis is flipped at the distance where the phase mismatch between the driving pulse and its propagating harmonic reaches $\pi$. So, instead of increasing from $\pi$ to 2 $\pi$, the phase mismatch increases from 0 to $\pi$ once again. However, it is impossible in HHG to create similar periodically poled laser plasmas for HHG because of the inversion symmetry of gaseous or plasma media, so an alternative

OPTICS CONTINUUM

approach to QPM is required. HHG QPM in laser plasmas and gases by temporal, or equally, more easily achieved spatial modulation of fields is based on the compensation of phase mismatch $\Delta\phi$ accumulated between the two fields with different frequencies (in HHG this is the driving field and its certain harmonics) when propagating in the dispersive medium.

The commonly accepted understanding of optimal HHG QPM is that the multijet structure of gas or plasma changes $\Delta\phi$ from $\pi$ at the exit from one jet to 2 $\pi$ at the beginning of another jet, so the separation between the jets prohibits the destructive generation of harmonics in opposite directions of the electric field when $\pi < \Delta\phi < 2\pi$. During HHG QPM the transition from plasma jets to no-plasma intervals is not as distinct, as, for example, the boundary between periodically poled crystal structures in classical QPM. The optical properties of no-plasma regions may also differ significantly from properties of plasma jets. Namely, the change of the phase at the exit of the jet is not necessarily $\pi$, but the total phase change of a harmonic after passing one jet and one no-plasma region is »2 $\pi$, which one can call the $2\pi$ QPM condition. This $2\pi$ QPM condition is currently assumed to support the experimentally observed near-quadratic growth of the HHG QPM efficiency with the number of jets.

Below we address the usefulness of the relation between the coherence length, maximally enhanced harmonic order, and electron density of LIP. According to Eq. (3), a 1.5-fold increase in $L_{\mathrm{coh}}$ should provide QPM for the 2/3 harmonic order. Particularly, changing plasma jet sizes from 0.4 mm (Fig. 4(b), middle panel) to 0.6 mm (Fig. 4(b), bottom panel) in the case of indium plasma should lead to the variation of the peak of harmonic distribution from H38 to H25. However, the observed peak was changed from H38 to H33.

The relation ($L_{\mathrm{coh}} \times q \propto$ const) is fulfilled once one uses the same concentration of the free electrons appearing during the over-excitation of a target. Meanwhile, the line-outs taken from the raw images presented in the middle and bottom parts of Fig. 4(b) are related to different conditions of extended plasma formation. In other words, these two spectra were not taken from the indium LIP by simple replacement of MSM by another one. In some cases, we initially optimized the extended (5-mm) plasma to further achieve the maximum harmonic yield from different multi-jet plasma structures. Particularly, it was done in the case of experiments with indium plasma. Because of this, the above relation was not maintained in the case of the data presented in Fig. 4(b) for the In multi-jet LIP.

Meanwhile, once we do not change the conditions of target ablation, the $L_{\mathrm{coh}} \times q_{\mathrm{max}}$ rule becomes closely followed. The confirmation of this feature can be seen in the case of Mn plasma (Figs. 5(b) and 5(c)). Contrary to experiments with indium plasma, these two spectra were taken from the manganese plasma at the same fluence of heating pulses. In that case, the multi-jet structures were formed by the simple replacement of one MSM by another one. The observation of maximally enhanced H43 in the case of 6-jet plasma allowed us to expect that in the case of 8-jet plasma the maximally enhanced order of QPM-enhanced harmonics would be 43×8:6~H57. Our experiment with 8-jet plasma confirmed this assumption: the maximally enhanced harmonic was H55.

Our studies underline how sensitive the process of QPM formation is in laser plasma. Even a small variation of the fluence of heating pulses allowed us to shift the maximally enhanced harmonic from expected H25 to H33 in the case of In LIP. Thus our studies showed another method of simultaneous modification of harmonics distribution by manipulation of both spatial and electron density parameters.

## 6. Conclusions

We compared two processes (resonance enhancement and quasi-phase-matching) that allow increasing the yield of the high-order harmonics of ultrashort pulses when propagating through various laser-induced plasmas. Vanadium, antimony, indium, and manganese plasmas were chosen as effective media for harmonic generation, where these processes either coincided

OPTICS CONTINUUM

spectrally or separated in the extreme ultraviolet range. We showed how the tuning of maximally enhanced harmonics during quasi-phase-matching in multi-jet plasma can increase the output of the resonance-enhanced single harmonic. Our experimental study is confirmed by the numerical calculations of QPM harmonics. We showed that adjusting the extended region of the photoemission spectra in multi-jet plasma towards the position of the resonantly enhanced harmonic can open up the possibility for additional enhancement of the resonant harmonic. We showed up to 30-fold harmonic enhancement under QPM conditions, as well as an extension of the harmonic cutoffs in some of the studied plasmas. The predominance of the QPM gain over the resonance gain is shown. The tuning of groups of harmonics enhanced by QPM in the direction of areas where resonant enhancement of one harmonic can be realized is demonstrated.

**Funding.** European Regional Development Fund (1.1.1.5/19/A/003); Russian Foundation for Basic Research (18-02-40014).

**Acknowledgement.** R.A.G. thanks H. Kuroda for providing the opportunity in using the laser facility.

**Disclosures.** The authors declare no conflicts of interest.

**Data availability.** Data underlying the results presented in this paper are not publicly available at this time but may be obtained from the authors upon reasonable request**.**

## References

1. T. Ozaki, L. B. Elouga Bom, R. Ganeev, J.-C. Kieffer, M. Suzuki, and H. Kuroda, "Intense harmonic generation from silver ablation," Laser Part. Beams **25**(2), 321–325 (2007).
2. L. B. Elouga Bom, F. Bouzid, F. Vidal, J.-C. Kieffer, and T. Ozaki, "Correlation of plasma ion densities and phase matching with the intensities of strong single high-order harmonics," J," Phys. B **41**(21), 215401 (2008).
3. H. Singhal, V. Arora, B. S. Rao, P. A. Naik, U. Chakravarty, R. A. Khan, and P. D. Gupta, "Dependence of high-order harmonic intensity on the length of preformed plasma plumes," Phys. Rev. A **79**(2), 023807 (2009).
4. L. B. Elouga Bom, S. Haessler, O. Gobert, M. Perdrix, F. Lepetit, J.-F. Hergott, B. Carré, T. Ozaki, and P. Salières, "Attosecond emission from chromium plasma," Opt. Express **19**(4), 3677–3683 (2011).
5. M. Kumar, H. Singhal, J. A. Chakera, P. A. Naik, R. A. Khan, and P. D. Gupta, "Study of the spatial coherence of high order harmonic radiation generated from preformed plasma plumes," J. Appl. Phys. **114**(3), 033112 (2013).
6. H. Singhal, P. A. Naik, M. Kumar, J. A. Chakera, and P. D. Gupta, "Enhanced coherent extreme ultraviolet emission through high order harmonic generation from plasma plumes containing nanoparticles," J. Appl. Phys. **115**(3), 033104 (2014).
7. N. Rosenthal and G. Marcus, "Discriminating between the role of phase matching and that of the single-atom response in resonance plasma-plume high-order harmonic generation," Phys. Rev. Lett. **115**(13), 133901 (2015).
8. M. Wostmann, L. Splitthoff, and H. Zacharias, "Control of quasi-phase-matching of high-harmonics in a spatially structured plasma," Opt. Express **26**(11), 14524 (2018).
9. M. Kumar, H. Singhal, and J. A. Chakera, "High order harmonic radiation source for multicolor extreme ultraviolet radiography of carbon plumes," J. Appl. Phys. **125**(15), 155902 (2019).
10. S. R. Konda, Y. H. Lai, and W. Li, "Investigation of high harmonic generation from laser ablated plumes of silver," J. Appl. Phys. **130**(1), 013101 (2021).
11. S. R. Konda, V. R. Soma, M. Banavoth, R. Ketavath, V. Mottamchetty, Y. H. Lai, and W. Li, "High harmonic generation from laser-induced plasmas of Ni-doped CsPbBr3 nanocrystals: implications for extreme ultraviolet light sources," ACS Appl. Nano Mater. **4**(8), 8292–8301 (2021).
12. R. A. Ganeev, M. Suzuki, M. Baba, H. Kuroda, and T. Ozaki, "Strong resonance enhancement of a single harmonic generated in the extreme ultraviolet range," Opt. Lett. **31**(11), 1699–1701 (2006).
13. V. Strelkov, "Role of autoionizing state in resonant high-order harmonic generation and attosecond pulse production," Phys. Rev. Lett. **104**(12), 123901 (2010).
14. E. S. Toma, P. Antoine, A. D. Bohan, and H. G. Muller, "Resonance-enhanced high-harmonic generation," J. Phys. B **32**(24), 5843–5852 (1999).
15. M. B. Gaarde and K. J. Schafer, "Enhancement of many high-order harmonics via a single multiphoton resonance," Phys. Rev. A **64**(1), 013820 (2001).
16. C. Figueira de Morisson Faria, R. Kopold, W. Becker, and J. M. Rost, "Resonant enhancements of high-order harmonic generation," Phys. Rev. A **65**(2), 023404 (2002).
17. D. B. Milošević, "Resonant high-order harmonic generation from plasma ablation: Laser intensity dependence of the harmonic intensity and phase," Phys. Rev. A **81**(2), 023802 (2010).
18. D. B. Milošević, "High-energy stimulated emission from plasma ablation pumped by resonant high-order harmonic generation," J," Phys. B **40**(17), 3367–3376 (2007).
19. J. Seres, V. S. Yakovlev, E. Seres, C. H. Streli, P. Wobrauschek, C. H. Spielmann, and F. Krausz, "Coherent superposition of laser-driven soft-X-ray harmonics from successive sources," Nat. Phys. **3**(12), 878–883 (2007).

20. A. Pirri, C. Corsi, and M. Bellini, "Enhancing the yield of high-order harmonics with an array of gas jets," Phys. Rev. A **78**(1), 011801 (2008).
21. V. Tosa, V. S. Yakovlev, and F. Krausz, "Generation of tunable isolated attosecond pulses in multi-jet systems," New J. Phys. **10**(2), 025016 (2008).
22. T. Fok, Ł. Węgrzyński, M. Kozlova, J. Nejdl, P. W. Wachulak, R. Jarocki, A. Bartnik, and H. Fiedorovicz, "High-order harmonic generation using a multi-jet gas puff target," Photonics Lett. Pol. **6**(1), 14–19 (2014).
23. S. Y. Stremoukhov and A. V. Andreev, "Quantum-mechanical elaboration for the description of low- and high-order harmonics generated by extended gas media: prospects to the efficiency enhancement in spatially modulated media," Laser Phys. **28**(3), 035403 (2018).
24. A. V. Andreev, S. Y. Stremoukhov, and O. A. Shoutova, "Light-induced anisotropy of atomic response: prospects for emission spectrum control," Eur. Phys. J. D **66**(1), 16 (2012).
25. A. V. Andreev, R. A. Ganeev, H. Kuroda, S. Y. Stremoukhov, and O. A. Shoutova, "High-order harmonic cut-off frequency in atomic silver irradiated by femtosecond laser pulses: theory and experiment," Eur. Phys. J. D **67**(1), 22 (2013).
26. S. Y. Stremoukhov, "Quasi-phase matching of high harmonics driven by mid–IR: Towards the efficiency drop compensation," J. Opt. Soc. Am. B **39**(4), 1203–1208 (2022).
27. A. M. Rubenchik, M. D. Feit, M. D. Perry, and J. T. Larsen, "Numerical simulation of ultra-short laser pulse energy deposition and bulk transport for material processing," Appl. Surf. Sci. **127-129**, 193–198 (1998).
28. L. B. Elouga Bom, J.-C. Kieffer, R. A. Ganeev, M. Suzuki, H. Kuroda, and T. Ozaki, "Influence of the main pulse and prepulse intensity on high-order harmonic generation in silver plasma ablation," Phys. Rev. A **75**(3), 033804 (2007).
29. R. A. Ganeev, L. B. Elouga Bom, T. Ozaki, and P. V. Redkin, "Maximizing the yield and cutoff of high-order harmonic generation from plasma plume," J. Opt. Soc. Am. B **24**(11), 2770–2778 (2007).
30. J. Stadler, R. Mikulla, and H.-R. Trebin, "IMD: a software package for molecular dynamics studies on parallel computers," Int. J. Mod. Phys. C **08**(05), 1131–1140 (1997).
31. J. Roth, F. G. éahler, and H.-R. Trebin, "A molecular dynamics, run with 5 180 116 000 particles," Int. J. Mod. Phys. C **11**(2), 317–322 (2000).
32. R. A. Ganeev, T. Witting, C. Hutchison, F. Frank, P. V. Redkin, W. A. Okell, D. Y. Lei, T. Roschuk, S. A. Maier, J. P. Marangos, and J. W. G. Tisch, "Enhanced high-order harmonic generation in a carbon ablation plume," Phys. Rev. A **85**(1), 015807 (2012).
33. A. H. Sheinfux, Z. Henis, M. Levin, and A. Zigler, "Plasma structures for quasiphase matched high harmonic generation," Appl. Phys. Lett. **98**(14), 141110 (2011).
34. C. Kan, N. H. Burnett, C. E. Capjack, and R. Rankin, "Coherent XUV generation from gases ionized by several cycle optical pulses," Phys. Rev. Lett. **79**(16), 2971–2974 (1997).
35. M. Suzuki, L. B. Elouga Bom, T. Ozaki, R. A. Ganeev, M. Baba, and H. Kuroda, "Seventy-first harmonic generation from doubly charged ions in preformed laser-ablation vanadium plume at 110 eV," Opt. Express **15**(7), 4112–4117 (2007).
36. M. V. Frolov, N. L. Manakov, A. A. Silaev, and N. V. Vvedenskii, "Analytic description of high-order harmonic generation by atoms in a two-color laser field," Phys. Rev. A **81**(6), 063407 (2010).
37. M. Tudorovskaya and M. Lein, "High-order harmonic generation in the presence of a resonance," Phys. Rev. A **84**(1), 013430 (2011).
38. M. Suzuki, M. Baba, H. Kuroda, R. A. Ganeev, and T. Ozaki, "Intense exact resonance enhancement of single-high-harmonic from an antimony ion by using Ti:sapphire laser at 37 nm," Opt. Express **15**(3), 1161–1166 (2007).
39. R. D'Arcy, J. T. Costello, C. McGuinnes, and G. O'Sullivan, "Discrete structure in the 4d photoabsorption spectrum of antimony and its ions," J," Phys. B **32**(20), 4859–4876 (1999).
40. G. Duffy and P. Dunne, "The photoabsorption spectrum of an indium laser produced plasma," J," Phys. B **34**(6), L173–L178 (2001).
41. Z. Abdelrahman, M. A. Khohlova, D. J. Walke, T. Witting, A. Zair, V. V. Strelkov, J. P. Marangos, and J. W. G. Tisch, "Chirp-control of resonant high-order harmonic generation in indium ablation plumes driven by intense few-cycle laser pulses," Opt. Express **26**(12), 15745 (2018).
42. R. A. Ganeev, T. Witting, C. Hutchison, F. Frank, M. Tudorovskaya, M. Lein, W. A. Okell, A. Zaïr, J. P. Marangos, and J. W. G. Tisch, "Isolated sub-fs XUV pulse generation in Mn plasma ablation," Opt. Express **20**(23), 25239–25248 (2012).
43. M. A. Fareed, V. V. Strelkov, M. Singh, N. Thire, S. Mondal, B. E. Schmidt, F. Legare, and T. Ozaki, "Harmonic generation from neutral manganese atoms in the vicinity of the giant autoionization resonance," Phys. Rev. Lett. **121**(2), 023201 (2018).
44. I. S. Wahyutama, T. Sato, and K. L. Ishikawa, "Time-dependent multiconfiguration self-consistent-field study on resonantly enhanced high-order harmonic generation from transition-metal elements," Phys. Rev. A **99**(6), 063420 (2019).
45. H. Kjeldsen, F. Folkmann, B. Kristensen, J. B. West, and J. E. Hansen, "Absolute cross section for photoionization of Mn+ in the 3p region," J," Phys. B **37**(6), 1321–1330 (2004).
46. R. A. Ganeev, "Controlling single harmonic enhancement in laser produced plasmas," J. Appl. Phys. **121**(13), 133108 (2017).

47. V. V. Strelkov, M. A. Khokhlova, and N. Yu Shubin, "High-order harmonic generation and Fano resonances," Phys. Rev. A **89**(5), 053833 (2014).
48. R. A. Ganeev, S. Y. Stremoukhov, A. V. Andreev, and A. S. Alnaser, "Application of quasi-phase matching concept for enhancement of high-order harmonics of ultrashort laser pulses in plasmas," Appl. Sci. **9**(8), 1701 (2019).